coatings

MDPI

Article

Thermal-Insulation Fillers' Influences on the Heating Resistance of PDMS-Based Aerogel Layer

Linlin Liu [1,†], Xinyi Zhang [1,†], Weizhen Li [1], Shuchuan Wang [2], Jihu Wang [1], Shirong Wang [2] and Jingxia Yang [1,*]

[1] College of Chemistry and Chemical Engineering, Shanghai University of Engineering Science, LongTeng Road 333, Shanghai 201620, China; 15364511674@163.com (L.L.); zxy167857@163.com (X.Z.); liweizhen@sues.edu.cn (W.L.); wangjihu@163.com (J.W.)

[2] T&H Chemicals Co., Ltd., Tangxi Industrial Zone, Quanzhou Luojiang District, Quanzhou 362011, China; 1223045135@njupt.edu.cn (S.W.); xh@xinhepaint.com (S.W.)

* Correspondence: jxyang@sues.edu.cn

† These authors contributed equally to this work.

Abstract: PDMS-based aerogel layers were synthesized as insulation layers by adopting mullite fiber (MF), hollow glass microspheres (HGM) and silica aerogel (SA) as the main fillers, and their loading amounts and content ratios were checked to investigate their effects on the thermal insulation properties in PDMS composites by thermal conductivity, thermal stability, and thermal insulation. The loading amount of nanofillers can significantly influence the insulation-layer performance, and the best performance with the lowest thermal conductivity of 0.0568 W/(m·K) was obtained by 10 wt% loading in PDMS with MF:SA:HGM = 2:2:1, which can achieve a temperature difference (ΔT) of 67 °C on a 200 °C hotplate. Moreover, the variation of the filler content ratios can also affect the thermal insulation behavior when the loading amount is fixed at 10 wt%, and the best thermal barrier performance can be found for the sample with more SA as the filler (MF:SA:HGM = 1:3:1). The formed sample had the best thermal stability and thermal insulation property, which can stand a 9 min flame test without burning by butane spray gun, and the backside of the sample showed ΔT > 500 °C for the whole test.

Keywords: aerogel; PDMS; thermal insulation; flexible layer; nanofillers

Citation: Liu, L.; Zhang, X.; Li, W.; Wang, S.; Wang, J.; Wang, S.; Yang, J. Thermal-Insulation Fillers' Influences on the Heating Resistance of PDMS-Based Aerogel Layer. *Coatings* **2024**, *14*, 976. https://doi.org/10.3390/coatings14080976

Academic Editor: Hyung-Ho Park

Received: 28 June 2024
Revised: 30 July 2024
Accepted: 31 July 2024
Published: 2 August 2024

1. Introduction

Thermal insulation materials have become one of the research hotspots in recent years [1–6], and the use of thermal insulation materials can effectively reduce energy loss and improve energy efficiency [7–10]. In addition, thermal insulation materials can also effectively solve the problem of thermal runaway of the core power battery in new energy vehicles, and how to improve the performance of thermal insulation materials has also become one of the problems that the battery industry needs to overcome. Because separating the lithium-ion battery modules with a highly efficient insulation layer effectively prohibits thermal runaway (TR) propagation, aerogel is considered to be an important candidate, as the aerogel materials have low density and strong thermal insulation capacity; thus, some researchers have adopted aerogel materials to prohibit TR within battery modules [11–13].

At present, aerogel is mainly used in aircraft cabin insulation materials, new energy vehicle battery packs, industrial heating, transmission pipelines, etc. As a typical representative of nanoporous thermal insulation materials in superthermal insulation materials, its porous structure and three-dimensional network structure can prolong the heat-transfer path in the material, so it can reduce the thermal conductivity of the material [14–17]. However, due to its brittleness, silica aerogel alone has poor mechanical properties, which makes it difficult to use in practical applications. To address this issue, aerogels were often embedded into various resins together with fiber-reinforced composites to form thermal insulation layers with enhanced mechanical properties. The thermal insulation

layer is generally composed of substrates, thermal insulation fillers, etc., and is formed by hot pressing or coating compounding. The substrates include epoxy resin [18–21], polyurethane resin [22–27], and silicone resin [28–31], and the thermal insulation fillers are generally materials with low density and low thermal conductivity, such as silica aerogel, insulating glass microspheres, mica sheets, and fiber materials. For example, Zhang et al. [32] prepared flexible silicon-based aerogel composites using methyltrimethoxysilane as a precursor, impregnated with ceramic fiber (CF, 2.25 ± 0.25 mm), by supercritical drying, which was used to inhibit the thermal runaway propagation of lithium batteries. However, the supercritical drying method is not suitable for industrial production, so researchers prefer to incorporate aerogel powders with other substrates and prepare thermal insulation materials by a molding process [30,33–35] by adding aerogel powders into the silicone resin. For instance, a PDMS matrix composed of flexible Si-bonds was selected to give flexibility to the silica aerogel-filled composites, and a pore restoration method was applied to maintain the silica aerogel powders' unique porous structure in the PDMS matrix in order to retain their low thermal conductivity [31]. The existing research shows that aerogels can effectively improve the thermal insulation efficiency of materials. At present, the way to increase the amount of aerogel in the substrate and the aerogel dispersion needs to be improved to overcome the agglomeration phenomenon. During the molding process, the dispersion and the loading amount of aerogel are very important because the location and amount of aerogel have close relationships to the heating resistance of the insulation layers. Moreover, the flexible aerogel layer, which is mainly used for thermal insulation of batteries/electronic devices to effectively prevent the battery thermal runaway problem, still needs more research to improve its thermal hinder behavior because the flexible substrate often exhibits weak high-temperature resistance and it is difficult to achieve the synergistic improvement of the temperature resistance, and the fragility of SiO_2 aerogel needs to be overcome by embedment into the flexible substrate [36].

In this work, PDMS resin was used as the substrate because it will not burn completely when it is exposed to fire but will form a thin silica layer on the surface, which can prevent the fire from spreading [37,38]. Nevertheless, pure PDMS, after high-temperature burning, will decompose and become pulverization, which cannot fully meet the requirements of the thermal insulation in batteries/electronic devices, so it is necessary to add the ablation-resistant fillers in the PDMS layers to improve their stability at high temperatures. Thus, the silica aerogel powder (SA), together with mullite fiber (MF) and hollow glass microspheres (HGM), are loaded into silicone resin (polydimethylsiloxane resin, PDMS) for the preparation of the flexible heat-resistance layer. The ratio and loading amount of SA: MF: HGM were changed during the preparation of the SA–PDMS layers and the layers' structure and thermal conductivity were monitored to check their influences on their heating-resistance performance.

2. Experimental Section

2.1. Materials

PDMS resins with different viscosities (750, 2000, 5000 cps) were purchased from Shandong Xingchi Chemical Company (Zibo, China). Tetraethyl silicate (TEOS, AR) was purchased from Shanghai Titan Technology Co., Ltd. (Shanghai, China). Mullite fiber (MF) was purchased from Deqing Orka Refractory Co., Ltd. (Huzhou, China), with a length of 3–5 μm. Hollow glass microspheres (HGM) were purchased from 3M China Co., Ltd. (Guangzhou, China), with a thermal conductivity of 0.038 W/(m·K). Wetting dispersant (BYK-154), anti-settling agent (BYK-190), and defoamer (BK-226) were purchased from Qianhai Ji Shengya Technology Co., Ltd. (Shenzhen, China). Silica aerogels (SA) were laboratory homemade by modified process reported before [39], with the thermal conductivity of 0.0257 W/(m·K) and density of 0.0888 g/cm^3.

2.2. Preparation of Insulation Layer

In order to improve the dispersion of insulation fillers, three different types of PDMS resins (750, 2000, 5000 cps) were used to tone the viscosity, with the ratio of 750 cps: 2000 cps: 5000 cps = 4:5:1. The preparation procedure for the flexible insulation layer is shown in Figure 1. The total loading of the insulation filler was calculated based on the weight percentage (wt%) of the total PDMS (as listed in Table 1).

In a typical procedure, the needed amounts of SA, HGM, and MF (according to Table 1) were added to 40 g of PDMS (750 cps) and stirred by a high-speed disperser to form a uniform mixture. Then, TEOS (5 g), anti-settling agent (1 g) and dispersant (1 g) were added and further stirred for 15 min at a speed of 100 r/min. After that, additional PDMS (50 g of 2000 cps and 10 g of 5000 cps) were added into the mixture and dispersed at 500 r/min for 15 min. Finally, the curing agent was added and quickly stirred at 500 r/min for 2 min before the mixed slurry was transferred into the polytetrafluoroethylene mold (8 cm × 12 cm × 0.5 cm). After curing for 6 h at room temperature, the flexible insulation layer was obtained by demolding. By altering the solid loading amount, the layers were named x%S-A@PDMS, in which the x (x = 5, 10, 15, 20) represented the solid content amount of the same component ratio (MF:SA:HGM = 2:2:1). Meanwhile, the sample named 10%S-y@PDMS (y = A, B, C, D) indicated the serial of samples with the same solid content amount (fixed at 10 wt% of PDMS), but the ratio of MF:SA:HGM was changed.

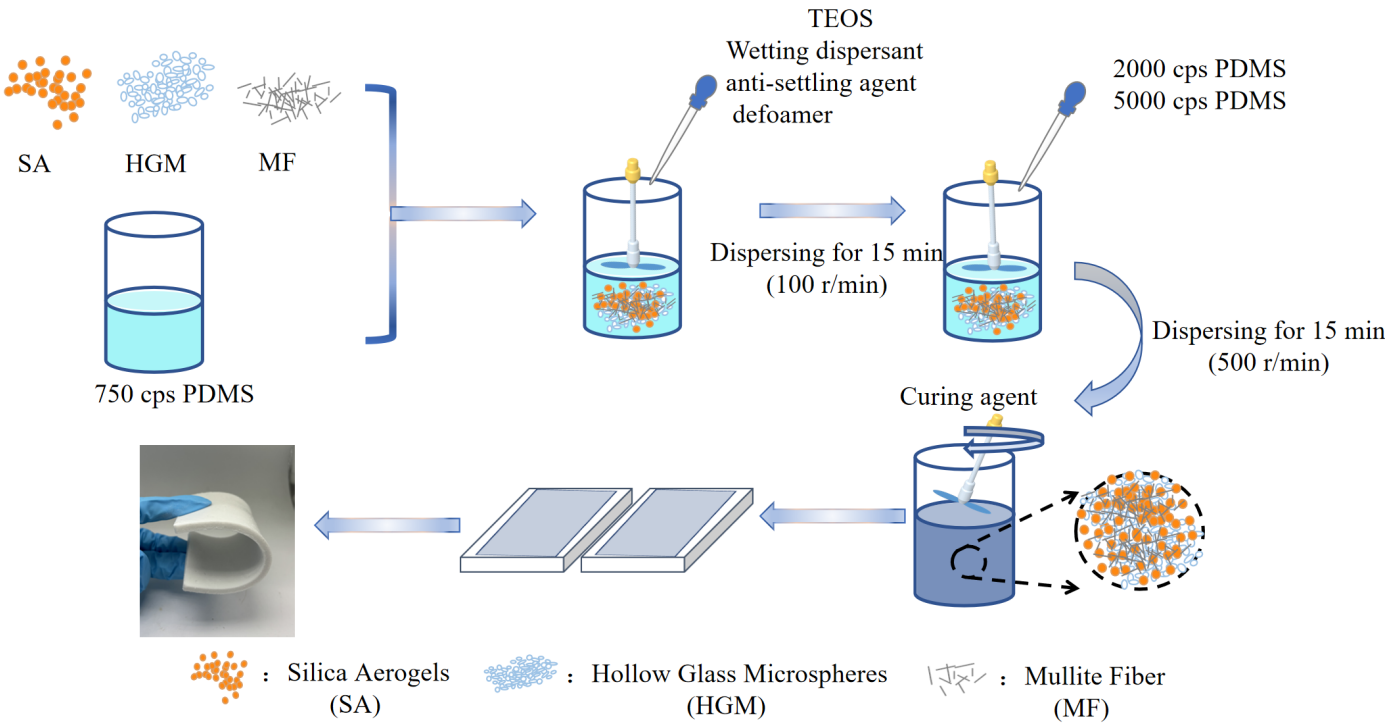

Figure 1. Preparation process of flexible insulation layer.

Table 1. Materials used for the preparation of flexible insulation layer.

Sample Name (MF:SA:HGM Ratio)	Sample Name								
	PDMS	MF	SA	HGM	TEOS	Wetting Dispersant	Anti-Settling	Defoamer	Curing Agent
5%S-A@PDMS (2:2:1)	100 g	2 g	2 g	1 g	5 g	1 g	1 g	1 g	4 g
10%S-A@PDMS (2:2:1)	100 g	4 g	4 g	2 g	5 g	1 g	1 g	1 g	4 g

Table 1. *Cont.*

Sample Name (MF:SA:HGM Ratio)	Sample Name								
	PDMS	MF	SA	HGM	TEOS	Wetting Dispersant	Anti-Settling	Defoamer	Curing Agent
15%S-A@PDMS (2:2:1)	100 g	6 g	6 g	3 g	5 g	1 g	1 g	1 g	4 g
20%S-A@PDMS (2:2:1)	100 g	8 g	8 g	4 g	5 g	1 g	1 g	1 g	4 g
10%S-B@PDMS (1:1:3)	100 g	2 g	2 g	6 g	5 g	1 g	1 g	1 g	4 g
10%S-C@PDMS (1:2:2)	100 g	2 g	4 g	4 g	5 g	1 g	1 g	1 g	4 g
10%S-D@PDMS (1:3:1)	100 g	2 g	6 g	2 g	5 g	1 g	1 g	1 g	4 g
10%S-MF@PDMS (5:0:0)	100 g	10 g	0 g	0 g	5 g	1 g	1 g	1 g	4 g
PDMS	100 g	0 g	0 g	0 g	5 g	1 g	1 g	1 g	4 g

2.3. Characterization

The surface morphology and structure of the samples were observed by a field emission scanning electron microscope (SEM, SU8010, Hitachi Company, Tokyo, Japan). The thermal conductivity meter (model: TC3000E, Xi'an Xiaxi Electronic Technology Co., Ltd., Xi'an, China) was used to test the thermal conductivity of the heat-insulation layer. The hardness of the insulation layer was measured by a Shore hardness tester (LX-A type). The thermal gravimetric (TG) curves of the samples were obtained using a simultaneous thermal analyzer (PerkinElmer, Waltham, MA, USA, STA 8000). The sample was photographed using a UTi32 infrared thermal imaging analyzer from unisex Technology and analyzed according to the temperature distribution.

The hydrophobicity characterization of the samples was obtained by contact angle measurement (JC2000D, Shanghai Zhongchen Digital Technology Equipment Co., Ltd., Shanghai, China). The measuring range was 0–180°, and the measuring accuracy was 0.01°. To test the water resistance, the material was also immersed in water for 24 h. The masses of the samples before and after immersion in water were recorded, and the water absorption of the insulation was calculated.

3. Results and Discussion

3.1. Loading Amount Influence of Insulation Fillers

In order to study the structure and morphology of the samples with different filler loadings, the SEM images of the samples' cross-section were checked (Figure 2). The pure PDMS exhibited a dense structure (Figure 2a). When the solid fillers were added into PDMS (Figure 2b–d), HGM structures with sphere structure could be observed clearly. Nevertheless, no clear SA particles and MF could be discerned. The cross-section of 10%S-A@PDMS showed the roughest surface, which may indicate good dispersion of solids in the PDMS matrix.

The effects of different solid contents on thermal conductivity, density, and Shore hardness of the insulating layer were measured, as shown in Figure 3. The Shore hardness of silicone resin is generally between 10 and 90 HA, and the high Shore hardness means the insulation layer has a strong resistance to external forces, which is good for practical application. The thermal conductivity of PDMS is 0.1047 W/(m·K) with a density of 0.92 g/cm^3 and a Shore hardness of 33 HA. After the loading of insulation fillers, the density and the thermal conductivity exhibited a concave structure trend, which decreased at first, but then increased with the percentage increase in the insulation filler, and 10%S-A@PDMS possessed the lowest density (0.63 g/cm^3) and thermal conductivity (0.0568 W/(m·K)). Although the Shore hardness (44 HA) of 10%S-A@PDMS was not as high as 47 HA of

20%S-A@PDMS, the value is reasonable for the insolation layer application in electronic components.

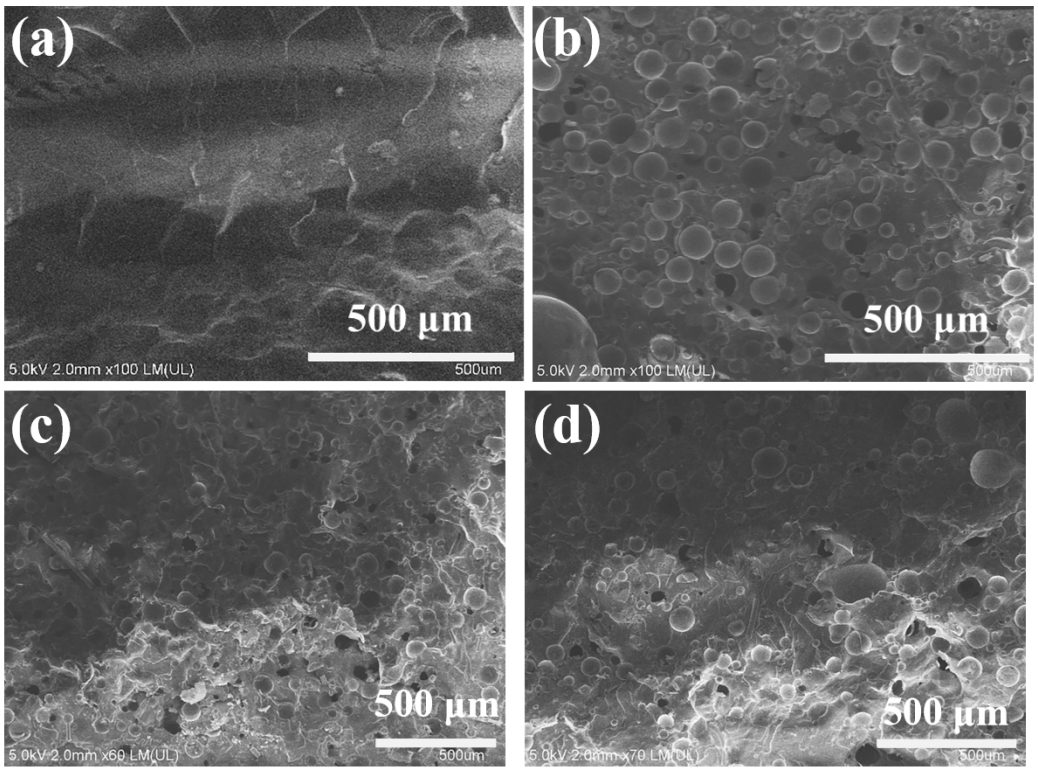

Figure 2. SEM image of sample cross-section (by liquid nitrogen quenching): (**a**) PDMS, (**b**) 5%S-A@PDMS, (**c**) 10%S-A@PDMS, and (**d**) 20%S-A@PDMS.

TGAs were used to test the thermal stability of the prepared insulation layer (Figure 4). For the pure PDMS sample, decomposition happened at 345 °C, and only one decomposition shoulder appeared, indicating the pure component in the materials. The decomposition behavior of the PDMS was similar to that in the literature [40]. After the loading of aerogel containing fillers, the decomposition slope shifted to a higher temperature, and an additional shoulder appeared at about 400 °C. This redshift indicated that the addition of insulation fillers had successfully hindered the heat conduction in the insulation layers, leading to a delayed temperature. The residual weight increased with the increase in the filler loading amount, from 33.17% to 48.90%.

The thermal insulation performance of x%S-A@PDMS samples was further checked by a heating experiment on a heating table. The heating table was set to 50 °C and 200 °C, respectively, and the front side of the x%S-A@PDMS samples was checked by an infrared thermal-imaging analyzer (Figure 5). When the heating table was set to 50 °C and heated for 5 min, the temperature difference (ΔT) between the upper surface of the PDMS sample and the heating platform was only 2 °C (Figure 5a_1). However, with the addition of solid additives, this ΔT value increased (Figure 5b_1–e_1), indicating that the thermal resistance improved. Nevertheless, the ΔT did not change a lot when the solid content reached and over 10 wt% (Figure 5c_1–e_1), and this phenomenon is similar to the 200 °C heating test (Figure 5b_2–e_2). This dramatically improved insulation ability can be attributed to the low conductivity and high thermal stability of the added insulation fillers (SA, MF, HGM), which were mostly formed by inorganic compounds such as SiO_2 or/and ZrO_2/Al_2O_3. Moreover, SA and HGM with porous or hollow structures can effectively hinder heat transfer, while the MF with a fiber structure provides mechanical properties. The biggest ΔT values were achieved when 10%S-A@PDMS was adopted as the insulation layer, which was 9.7 °C (Figure 5c_1, hotplate: 50 °C) and 64 °C (Figure 5c_2, hotplate: 200 °C). When the

temperature of the front layers was recorded along with the time (Figure 5f,g), the results confirmed that the 10%S-A@PDMS had the best performance, and the further increase in the solid filler cannot improve the heating resistance significantly, which may be because the overloaded solid materials blocked some pores, which reduced the thermal barrier effect. Meanwhile, more MF existed in the samples with high solid loading, which accelerated heat transfer by its fiber structure. Thus, in the following investigation, the solid content was fixed at 10 wt% to study the filler content influence on the heating-barrier performance.

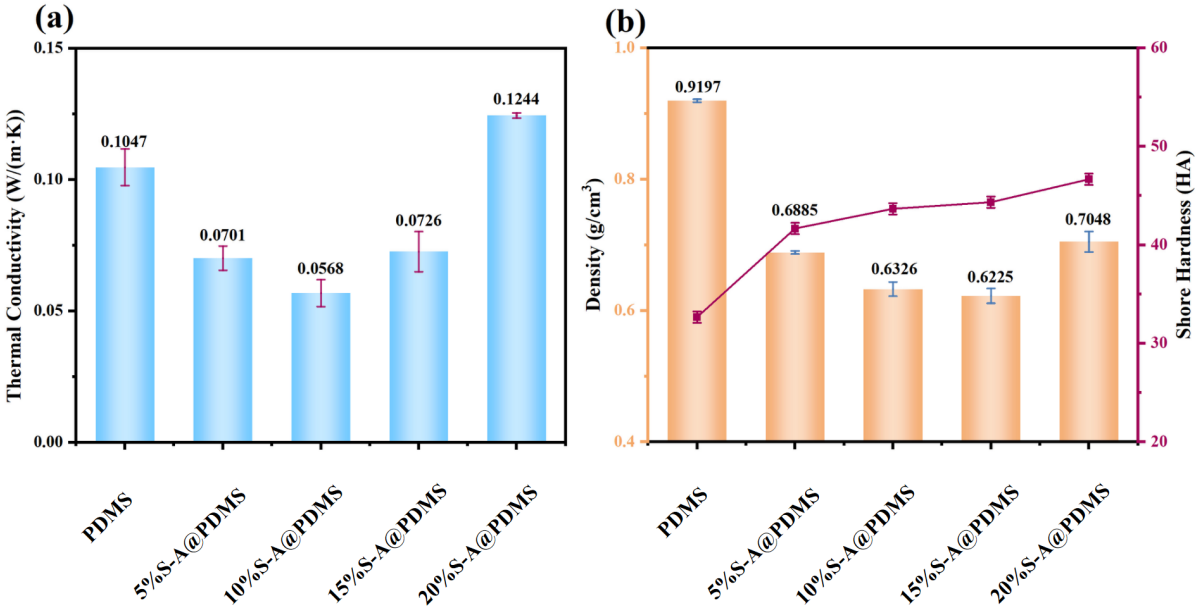

Figure 3. (**a**) Thermal conductivity and (**b**) density, Shore hardness of PDMS and x%S-A@PDMS.

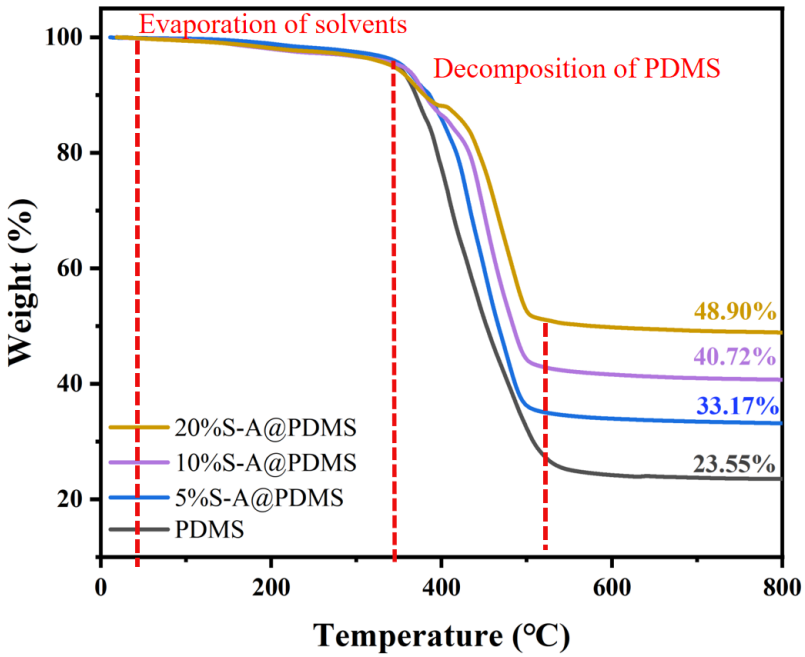

Figure 4. Thermogravimetric analysis curve of pure PDMS, 5%S-A@PDMS, 10%S-A@PDMS, and 20%S-A@PDMS.

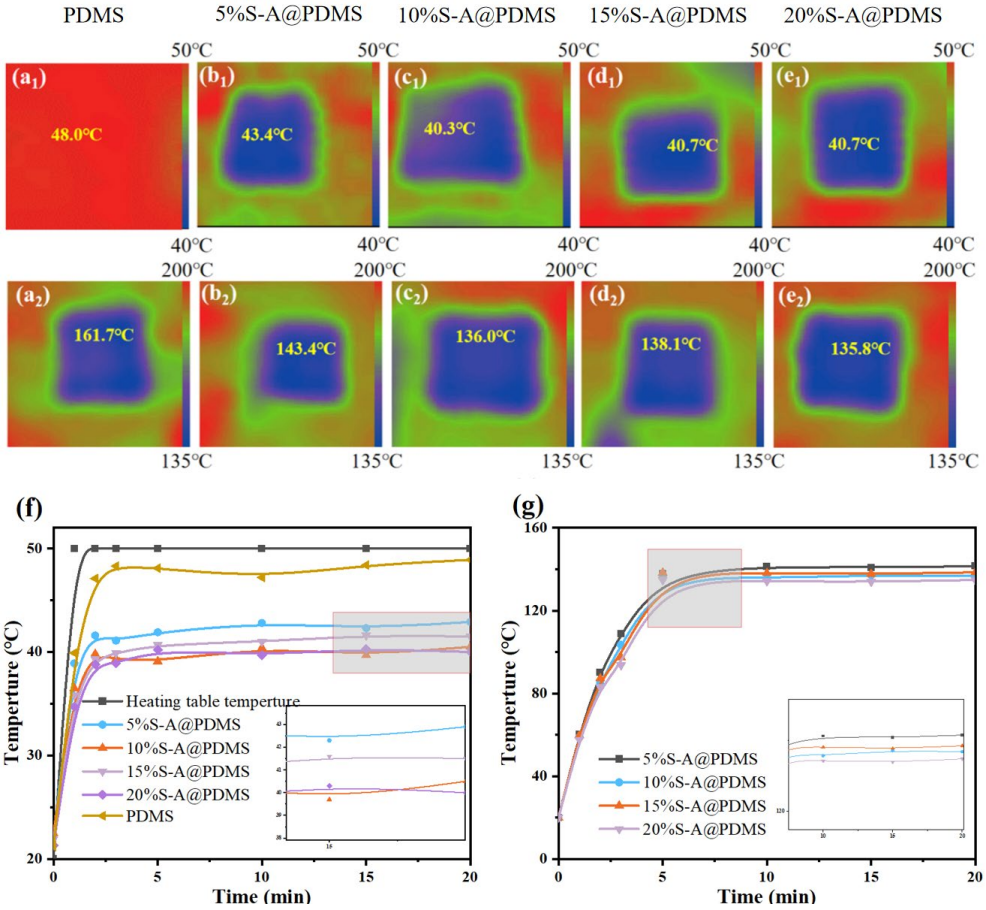

Figure 5. Thermal images of PDMS (**a1**,**a2**) and x%S-A@PDMS(**b1**–**e1**,**b2**–**e2**) heated at 50 °C and 200 °C for 5 min on heating tables (insulation thickness is 2 mm), (**f**,**g**) the top surface temperature of PDMS and x%S-A@PDMS changes with time at 50 °C (**f**) and 200 °C (**g**) on a heating table.

3.2. Component Influence of Insulation Fillers

Samples with the fixed 10 wt% nanofillers but different contents were characterized by thermal conductivity, density, and Shore hardness (Figure 6a,b). Meanwhile, the sample only containing MF (10%S-MF@PDMS) as barriers were also checked. All samples containing SA and HGM (10%S-A/B/C/D@PDMS) exhibited lower thermal conductivity (0.0568–0.0861 W/(m·K)) and lower density (0.6160–0.6326 g/cm^3) than the 10%S-MF@PDMS sample (0.1201 W/(m·K)) with a density of 0.7145 g/cm^3. Basically, the thermal conductivity decreased with the increase in the SA component (10%S-B/C/D@PDMS) and did not change too much when the SA content was 4~6 g in the insulation layer (sample 10%S-A/C/D@PDMS). Moreover, when the cross-sectional SEM images were checked for 10%S-MF@PDMS (Figure 6c) and 10%S-D@PDMS (Figure 6d), a lot of pore and sphere structures could be found in 10%S-D@PDMS (with MF:SA:HGM = 1:3:1), while the surface was relatively flat for 10%S-MF@PDMS. Although the SA structure could not be discerned due to the tiny pore structure, the SA's loose skeleton structure and the hollow structure of HGM can extend the heat-transfer path, enhancing thermal insulation [41]. The Shore hardness of the samples (10%S-A/B/C/D@PDMS) were 43–44 HA, which was slightly higher than that of the 10%S-MF@PDMS sample (40 HA), indicating that the addition of the insulation fillers could enhance the ability of the insulation layer to resist external damage.

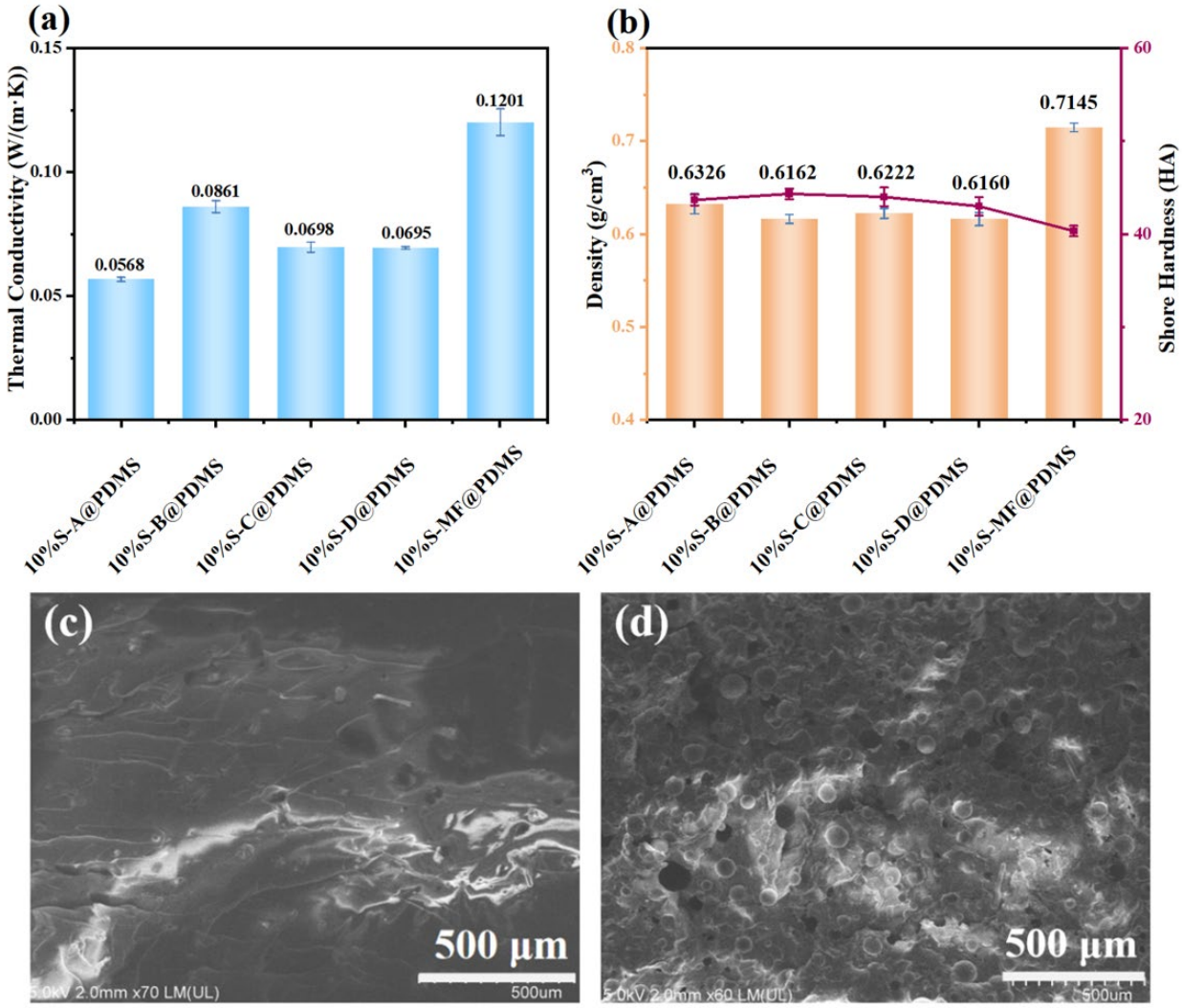

Figure 6. (**a**) Thermal conductivity, (**b**) density, and Shore hardness of 10%S-A, B, C, D, MF@PDMS insulation coating (A sample (MF:SA:HGM = 2:2:1), B sample (MF:SA:HGM = 1:1:3), C sample (MF:SA:HGM = 1:2:2), D sample (MF:SA:HGM = 1:3:1)), SEM image of liquid nitrogen quenching of (**c**) 10%S-MF@PDMS and (**d**) 10%S-D@PDMS.

The contact angle (CA) of the sample with different barriers was explored, as shown in Figure 7a. The CA of the PDMS sample is 115.5° (Figure 7a), indicating that the silicone resin itself is a hydrophobic material with good properties. The addition of heat-insulation fillers caused the CA to slightly increase, and the contact angle of the 10%S-D@PDMS sample is 122.0° (Figure 7d). Furthermore, the water resistance was tested by immersing the samples in water for 24 h. Table 2 shows the masses of the samples before and after immersion in water, and the water absorption of the insulation was calculated. The PDMS sample had the highest absorption rate at 3.8%, indicating the layer had good water resistance (Figure 7e). Moreover, 10%S-A@PDMS and 10%S-D@PDMS samples showed even lower absorption rates at 1.4% and 1.1%, respectively. The water absorption decreased with the increase of SA, probably due to the hydrophobic methyl groups in SA, which inhibit water penetration. Thus, adding SA improves the water resistance of the thermal insulation coating, mitigating the effects of moisture.

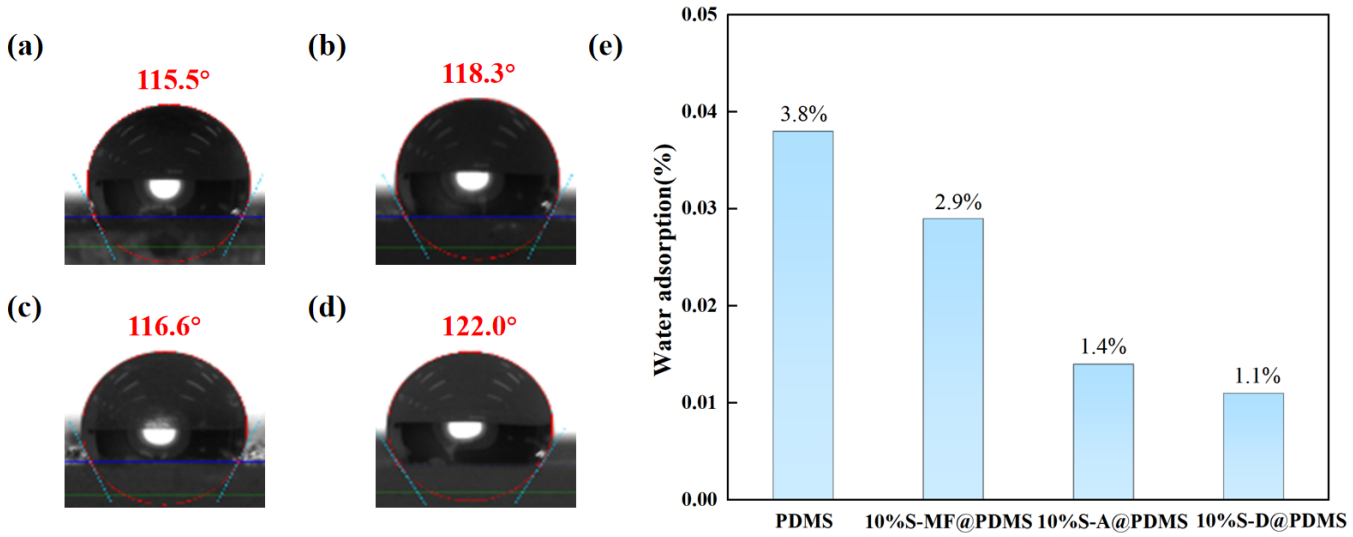

Figure 7. Water contact angles of the sample surface of (**a**) PDMS, (**b**) 10%S-MF@PDMS, (**c**) 10%S-A@PDMS, and (**d**) 10%S-D@PDMS. (**e**) Water adsorption of PDMS, 10%S-MF@PDMS, 10%S-A@PDMS, and 10%S-D@PDMS.

Table 2. Water adsorption of PDMS, 10%S-MF@PDMS, 10%S-A@PDMS, and 10%S-D@PDMS.

Sample	Pre-Soaking (m_0) (g)	Post Soaking (m_1) (g)	Water Adsorption $((m_1 - m_0)/m_0 \times 100\%)$ (%)
PDMS	15.73	16.32	3.8%
10%S-MF@PDMS	12.22	12.57	2.9%
10%S-A@PDMS	10.82	10.97	1.4%
10%S-D@PDMS	10.54	10.66	1.1%

The infrared thermal images of thermal insulation layers with varying proportions of solid filling materials on heating platforms (50 °C and 200 °C, respectively) are shown in Figure 8. The images reveal that the heat-blocking effect improves with the aerogel content increasing (10%S-B@PDMS: 2 g, 10%S-C@PDMS: 4 g and 10%S-D@PDMS: 6 g). Specifically, the upper surface temperature of the 10%S-D@PDMS sample was 37.9 °C after being placed on a 50 °C heating platform for 5 min and 132.7 °C after being heated on a 200 °C platform for 5 min. Compared to the 10%S-B@PDMS sample with the lowest aerogel content, the upper surface temperatures of 10%S-D@PDMS were reduced by 3 °C and 8.2 °C, respectively. These results are consistent with the thermal conductivity measurements of the insulation layers, indicating that the addition of SA can enhance the material's thermal insulation properties.

The resistances of the samples were also confirmed by a heat-treatment test (Figure 9a–c) and an ablation test (Figure 9d–f). For the heat-treatment test, the samples were heat-treated in a Muffle oven at 300 °C and 400 °C for 1 h, respectively. Although all samples exhibited a white color before heat treatment (Figure 9a), the surface turned to yellow after a 300 °C treatment for 1 h, and 5%S-A@PDMS (MF:SA:HGM = 2:2:1) showed the deepest color change. In contrast, the 10%S-D@PDMS sample (MF:SA:HGM = 1:3:1) showed the lightest yellow color, indicating it had the best heating resistance (Figure 9b). The same trend can be found after the 400 °C heating; 10%S-D@PDMS only exhibited color change, while the other two samples showed blistering or coking (Figure 9c). The color change was most related to the structure change of the silicone resin. The most SA loading, which was in 10%S-D@PDMS, can effectively hinder the heating conductivity in the layer, resulting in the highest heating-resistance performance. Thus, the 10%S-D@PDMS was further used to carry out an ablation test by a butane spray gun (Figure 9d,e), and the sample bent when exposed to the flame, forming a lamellar structure

that fell off under continuous butane torch combustion. This structure was probably a thin silicon dioxide layer formed from burning silicone, which, despite poor mechanical properties, tends to prevent fire spread. Figure 9f shows the burn point and the backboard for the 10%S-D@PDMS sample during the ablation test. The backboard temperature reached 365 °C after 4 min and increased to 365 °C after 6 min, and it finally remained at 405 °C for 9 min without burning. The temperature difference between the burn point and the backboard was over 500 °C, confirming the good heating resistance of the 10%S-D@PDMS sample.

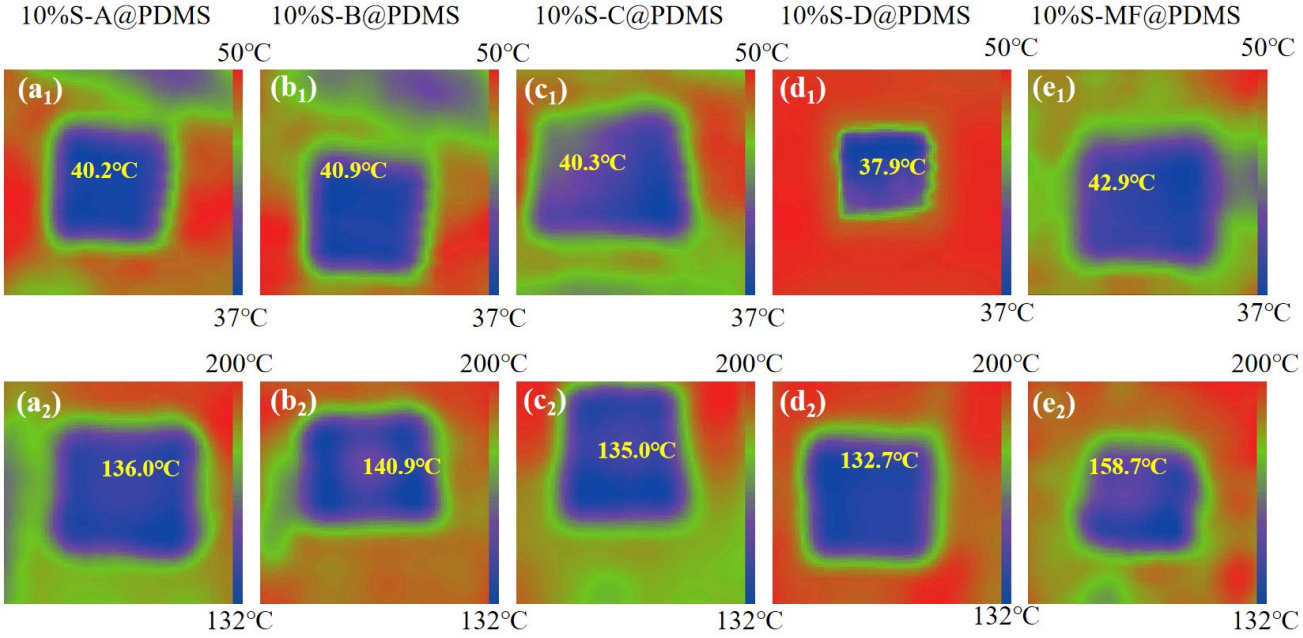

Figure 8. Thermal images of 10%S-A, B, C, D@PDMS ($\mathbf{a_1}$–$\mathbf{d_1}$,$\mathbf{a_2}$–$\mathbf{d_2}$) and 10%S-MF@PDMS($\mathbf{e_1}$,$\mathbf{e_2}$) at 50 °C and 200 °C for 5 min on heating tables (thickness of insulation layer is 2 mm).

Figure 10 illustrates the tensile stress–strain curves and the breaking strengths, and the tensile strength of 10%S-x@PDMS is greater than that of pure PDMS. Specifically, the tensile strength of 10%S-D@PDMS increased to 0.6 MPa, while pure PDMS is less than 0.2 MPa. Moreover, the tensile strength of 10%S-D@PDMS is 0.4 MPa higher than that of 10%S-MF@PDMS. Furthermore, the elongation at break of sample 10%S-D@PDMS decreased to 21.79%, which is about 20% less than that (49.1%) of PDMS. Although the mechanical properties of the samples are not excellent, they meet the requirements for thermal insulation application in batteries and electronic equipment (tensile strength $\geq$ 0.5 MPa from T/CSTM 00193-2020 "Aerogel Insulation Sheet for Lithium-ion Power Battery").

The comparison of insulation properties for sample 10%S-A@PDMS with references are summarized in Table 3. The temperature difference per unit layer thickness ΔT_u (°C/mm) was used to indicate the performance of the insulation layers. It can be seen that sample 10%S-A@PDMS is good compared to the other samples, with ΔT_u of 32 °C/mm. Although the performance of 10%S-A@PDMS was not the best compared with the literature results, its properties are still outstanding compared to the related aerogel samples.

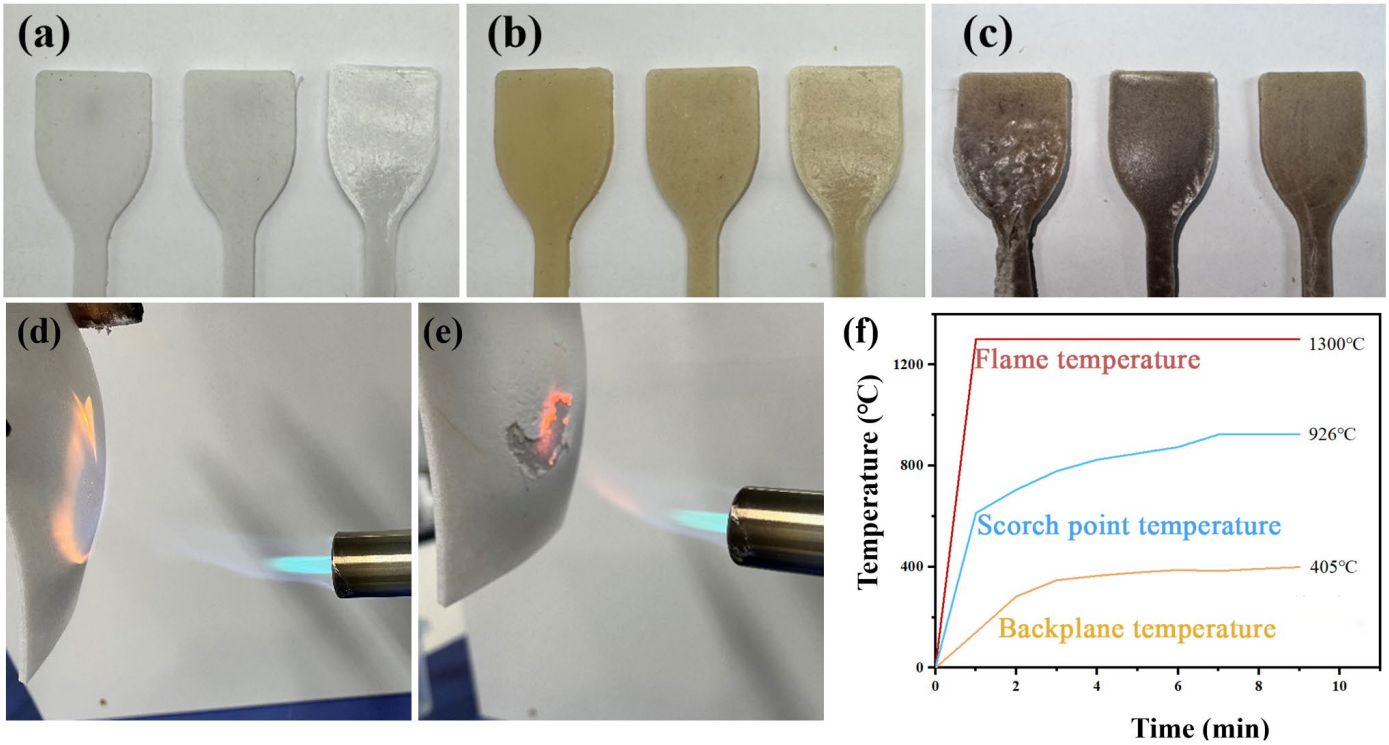

Figure 9. Digital picture of 5%S-A@PDMS, 10%S-A@PDMS, and 10%S-D@PDMS (from left to right) after heat treatment in Muffle furnace: (**a**) as-prepared, (**b**) 300 °C, 1 h; (**c**) 400 °C, 1 h. (**d**–**f**) Digital images of 10%S-D@PDMS before and after ablation: (**d**) at the beginning of the burn, (**e**) 10 min after the burn, (**f**) temperature curve of burning point and backplane during 10%S-D@PDMS ablation test.

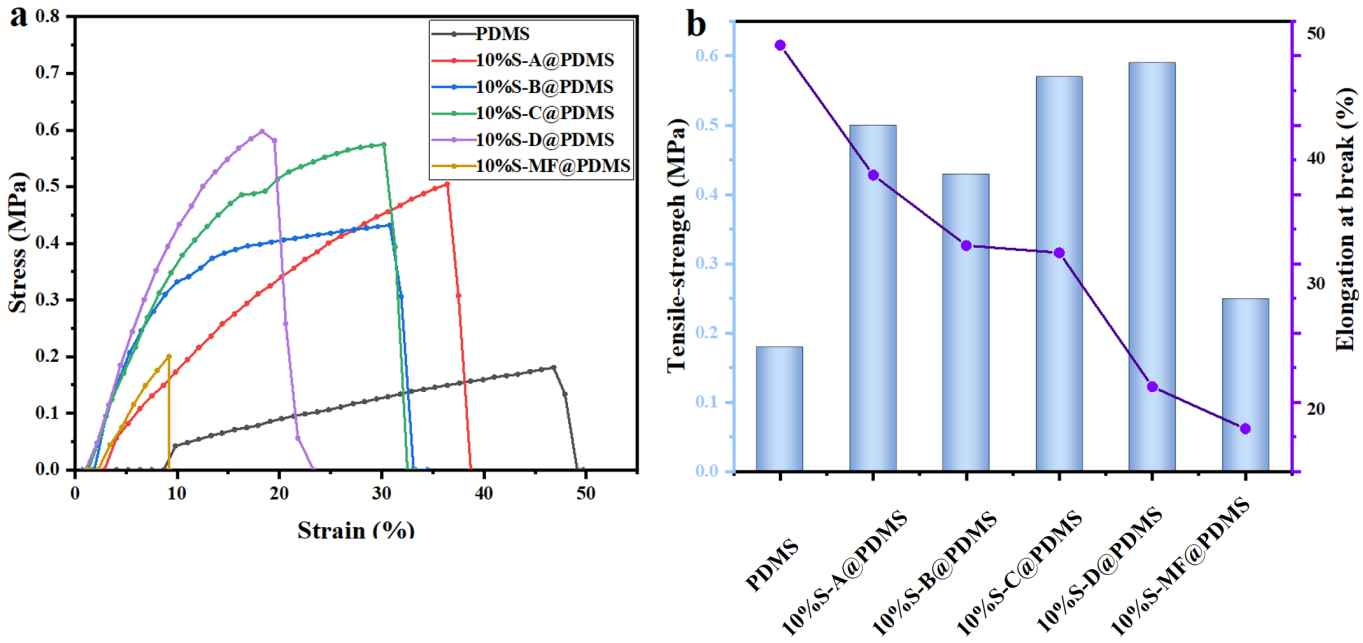

Figure 10. (**a**) Stress–strain curve for 10%S-x@PDMS, (**b**) tensile properties of different samples: tensile strength and elongation at break.

Table 3. Comparison of sample insulation properties.

Sample Name	Aerogel Content (wt%)	Matrix	Thermal Conductivity (W/(m·K))	Density (g/cm^3)	Temperature of Hot Table (°C)	Temperature Difference ΔT between up and down Sides (°C)	Thickness of Sample (mm)	Calibrated ΔT_u per Unit Thickness (°C/mm)	Reference
10%S-A@PDMS	4	PDMS	0.0568	0.6236	200	64	2	32	This study
C6	6	styrene-acrylic latex	0.05748	/	400	163	4	40.75	2023 [42]
SCSA-HGMs	2	CSA	0.065	/	200	138.5	15	10.87	2023 [43]
CABs	1	CAB	0.053	/	150	94.2	8	11.7	2022 [31]
C6	6	β-SiC	0.057	/	1100	710	10	71	2024 [44]
15 wt% SA	15	SiO_2	0.0303	/	500	420.1	15	28	2023 [45]

The heat-transfer mechanism of the flexible insulation layer is illustrated in Figure 11. The solid filler materials evenly distribute and encapsulate heat in the silicone resin. When a heat source approaches, the heat enters from one side of the insulation layer, and for 10%S-MF@PDMS, although MF can enhance the mechanical property (Shore hardness: 40 HA) compared with pure PDMS (Shore hardness: 33 HA), the heating resistance is not as good as those containing more SA in the layer. Inside the 10%S-D@PDMS insulation layer, aerogel, hollow glass beads, and mullite short fibers form an intricate cross-linked network, creating numerous pores (Figure 10b). Specifically, the pore size of the aerogel is smaller than the average molecular free path of air (≤70 nm), effectively preventing free airflow and restraining heat convection. This reduces the heat-conduction capability of the insulation layer, thereby lowering its thermal conductivity. Additionally, the loose structure of the aerogel extends the heat-transfer path, further enhancing the thermal insulation properties of the system and ultimately slowing down the heat transfer to the other side.

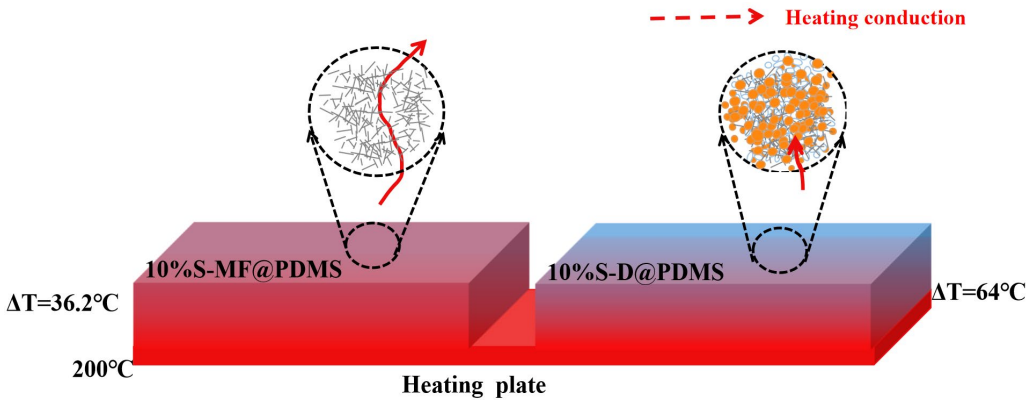

Figure 11. Schematic diagram of heat-transfer mechanism of flexible insulation layer.

4. Conclusions

Mullite fiber (MF), hollow glass microspheres (HGM), and silica aerogels (SA) were used as heat-barrier fillers in PDMS resin, and the formed flexible insulation layers were checked by thermal conductivity, thermal stability, and thermal insulation properties. The influences of the loading amounts and component ratios of the fillers were investigated. When the component ratio was fixed at MF:SA:HGM = 2:2:1, the filler loading amount can be changed within the range of 5~20 wt% of PDMS resin, and the one with 10 wt% exhibited the lowest thermal conductivity of 0.0568 W/(m·K), with an upper surface temperature of 136 °C on a 200 °C hotplate. Moreover, with the loading amount fixed at 10 wt% of PDMS resin, the higher ratio of SA in the filler yielded a flexible layer with higher thermal insulation properties, and the best sample, 10%S-D@PDMS, with MF:SA:HGM = 1:3:1, showed the best heat stability, which had no coke after being heated at 400 °C for 1 h. Moreover, the ablation test by butane spray gun for 10%S-D@PDMS suggested that the sample had very good thermal barriers, which showed a temperature difference of over 500 °C after a 9 min flame test. The SA porous structure played an important role in the thermal insulation.

Author Contributions: Methodology, W.L.; Validation, S.W. (Shuchuan Wang); Formal analysis, L.L.; Investigation, X.Z.; Resources, J.W.; Data curation, X.Z.; Writing—original draft, L.L.; Writing—review & editing, J.Y.; Supervision, J.Y.; Project administration, S.W. (Shirong Wang). All authors have read and agreed to the published version of the manuscript.

Funding: This research is supported by the Natural Science Foundation of Shanghai (No. 23ZR1425700) and the College Student Research Training Program of SUES (No. cx2404006).

Institutional Review Board Statement: Not applicable.

Informed Consent Statement: Not applicable.

Data Availability Statement: Data are contained within the article.

Acknowledgments: Thanks to the support of Class III Peak Discipline of Shanghai—Materials Science and Engineering (High-Energy Beam Intelligent Processing and Green Manufacturing). Thanks to Wuyu Yao, Tongyu Yang, Fan Xu and Yu Fu for the material preparing.

Conflicts of Interest: Shuchuan Wang and Shirong Wang are employed by T&H Chemicals Co., Ltd. The funders had no role in the design of the study; in the collection, analyses, or interpretation of data; in the writing of the manuscript; or in the decision to publish the results.

References

1. Shen, X.; Mao, T.; Li, C.; Mao, F.; Xue, Z.; Xu, G.; Amirfazli, A. Durable superhydrophobic coatings based on CNTs-SiO_2gel hybrids for anti-corrosion and thermal insulation. *Prog. Org. Coat.* **2023**, *181*, 107602. [CrossRef]
2. Wang, D.Y.; Liu, L.; Liu, Y.B.; Li, T.; Ma, Z.; Wu, H.X. Heat insulating capacity of $Sm_2Zr_2O_7$ coating added with high absorptivity solids. *Ceram. Int.* **2017**, *43*, 2884–2887. [CrossRef]
3. Pan, Y.; Han, D.; Huang, S.; Niu, Y.; Liang, B.; Zheng, X. Thermal insulation performance and thermal shock resistance of plasma-sprayed TiAlCrY/$Gd_2Zr_2O_7$ thermal barrier coating on γ-TiAl alloy. *Surf. Coat. Technol.* **2023**, *468*, 129715–129716. [CrossRef]
4. Sun, G.; Yang, L.; Liu, R. Thermal insulation coatings based on microporous particles from Pickering emulsion polymerization. *Prog. Org. Coat.* **2021**, *151*, 106023. [CrossRef]
5. Lakatos, A.; Lucchi, E. Thermal performances of Super Insulation Materials (SIMs): A comprehensive analysis of characteristics, heat transfer mechanisms, laboratory tests, and experimental comparisons. *Int. Commun. Heat Mass Transf.* **2024**, *152*, 107293. [CrossRef]
6. Acar, G.; Steeman, M.; Van Den Bossche, N. Reusing Thermal Insulation Materials: Reuse Potential and Durability Assessment of Stone Wool Insulation in Flat Roofs. *Sustainability* **2024**, *16*, 1657. [CrossRef]
7. Mao, T.; Li, C.; Mao, F.; Xue, Z.; Xu, G.; Amirfazli, A. A durable anti-corrosion superhydrophobic coating based on carbon nanotubes and SiO_2 aerogel for superior protection for Q235 steel. *Diam. Relat. Mater.* **2022**, *129*, 109370. [CrossRef]
8. Becker, P.F.B.; Effting, C.; Schackow, A. Lightweight thermal insulating coating mortars with aerogel, EPS, and vermiculite for energy conservation in buildings. *Cem. Concr. Compos.* **2022**, *125*, 104283–104296. [CrossRef]
9. Cuce, E.; Cuce, P.M.; Wood, C.J.; Riffat, S.B. Toward aerogel based thermal superinsulation in buildings: A comprehensive review. *Renew. Sustain. Energy Rev.* **2014**, *34*, 273–299. [CrossRef]
10. Cuce, E.; Cuce, P.M.; Wood, C.J.; Riffat, S.B. Optimizing insulation thickness and analysing environmental impacts of aerogel-based thermal superinsulation in buildings. *Energy Build.* **2014**, *77*, 28–39. [CrossRef]
11. Liu, F.; Wang, J.; Yang, N.; Wang, F.; Chen, Y.; Lu, D.; Liu, H.; Du, Q.; Ren, X.; Shi, M. Experimental study on the alleviation of thermal runaway propagation from an overcharged lithium-ion battery module using different thermal insulation layers. *Energy* **2022**, *257*, 124768. [CrossRef]
12. Marlière, C.; Despetis, F.; Etienne, P.; Woignier, T.; Dieudonné, P.; Phalippou, J. Very large-scale structures in sintered silica aerogels as evidenced by atomic force microscopy and ultra-small angle X-ray scattering experiments. *J. Non-Cryst. Solids* **2001**, *285*, 148–153. [CrossRef]
13. Xiao, Y.; Yan, M.; Shi, L.; Gong, L.; Cheng, X.; Zhang, H.; Pan, Y. High-temperature resistant, super elastic aerogel sheet prepared based on in-situ supercritical separation method for thermal runaway prohibition of lithium-ion batteries. *Energy Storage Mater.* **2023**, *61*, 102871. [CrossRef]
14. Chang, X.; Cheng, X.; Zhang, H.; Li, W.; He, L.; Yin, X.; Liu, X.; Yu, J.; Liu, Y.-T.; Ding, B. Superelastic Carbon Aerogels: An Emerging Material for Advanced Thermal Protection in Extreme Environments. *Adv. Funct. Mater.* **2023**, *33*, 2215168. [CrossRef]
15. Lin, X.-C.; Li, S.-L.; Li, W.-X.; Wang, Z.-H.; Zhang, J.-Y.; Liu, B.-W.; Fu, T.; Zhao, H.-B.; Wang, Y.-Z. Thermo-Responsive Self-Ceramifiable Robust Aerogel with Exceptional Strengthening and Thermal Insulating Performance at Ultrahigh Temperatures. *Adv. Funct. Mater.* **2023**, *33*, 2214913. [CrossRef]
16. Liu, P.; Gao, H.; Chen, X.; Chen, D.; Lv, J.; Han, M.; Cheng, P.; Wang, G. In situ one-step construction of monolithic silica aerogel-based composite phase change materials for thermal protection. *Compos. Part B-Eng.* **2020**, *195*, 108072. [CrossRef]
17. Yang, J.; Wu, H.; Huang, G.; Liang, Y.; Liao, Y. Modeling and coupling effect evaluation of thermal conductivity of ternary opacifier/fiber/aerogel composites for super-thermal insulation. *Mater. Des.* **2017**, *133*, 224–236. [CrossRef]
18. Kucharek, M.; MacRae, W.; Yang, L. Investigation of the effects of silica aerogel particles on thermal and mechanical properties of epoxy composites. *Compos. Part A-Appl. Sci. Manuf.* **2020**, *139*, 106108. [CrossRef]
19. Maghsoudi, K.; Motahari, S. Mechanical, thermal, and hydrophobic properties of silica aerogel-epoxy composites. *J. Appl. Polym. Sci.* **2018**, *135*, 45706. [CrossRef]
20. Salimian, S.; Zadhoush, A.; Talebi, Z.; Fischer, B.; Winiger, P.; Winnefeld, F.; Zhao, S.; Barbezat, M.; Koebel, M.M.; Malfait, W.J. Silica Aerogel-Epoxy Nanocomposites: Understanding Epoxy Reinforcement in Terms of Aerogel Surface Chemistry and Epoxy-Silica Interface Compatibility. *ACS Appl. Nano Mater.* **2018**, *1*, 4179–4189. [CrossRef]
21. Krishnaswamy, S.; Bhattacharyya, D.; Abhyankar, H.; Marchante, V.; Huang, Z.; Brighton, J. Morphological, optical and thermal characterisation of aerogel-epoxy composites for enhanced thermal insulation. *J. Compos. Mater.* **2019**, *53*, 909–923. [CrossRef]

22. Cho, J.; Jang, H.G.; Kim, S.Y.; Yang, B. Flexible and coatable insulating silica aerogel/polyurethane composites via soft segment control. *Compos. Sci. Technol.* **2019**, *171*, 244–251. [CrossRef]
23. Merillas, B.; Lamy-Mendes, A.; Villafane, F.; Duraes, L.; Angel Rodriguez-Perez, M. Silica-Based Aerogel Composites Reinforced with Reticulated Polyurethane Foams: Thermal and Mechanical Properties. *Gels* **2022**, *8*, 392. [CrossRef]
24. Merillas, B.; Lamy-Mendes, A.; Villafane, F.; Duraes, L.; Rodriguez-Perez, M.A. Polyurethane foam scaffold for silica aerogels: Effect of cell size on the mechanical properties and thermal insulation. *Mater. Today Chem.* **2022**, *26*, 101257. [CrossRef]
25. Nuhu, I.; Halim, Z.A.A.; Awang, N.; Yajid, M.A.M.; Ali, W.F.F.W. Fabrication and Characterization of Thermally Insulating Polyurethane-Silica Aerogel Composite for Cryogenic Application. *Silicon* **2024**, *16*, 2933–2944. [CrossRef]
26. Yin, R.; Cheng, H.; Hong, C.; Zhang, X. Synthesis and characterization of novel phenolic resin/silicone hybrid aerogel composites with enhanced thermal, mechanical and ablative properties. *Compos. Part A-Appl. Sci. Manuf.* **2017**, *101*, 500–510. [CrossRef]
27. Hao, G.; Li, X.; Wang, S.; Wang, S.; Ryu, M.; Yang, J. Surface Modification of Carbon Nanotubes in Silicone-Polyurethane for Improved Mechanical and Anticorrosion Properties. *Coatings* **2023**, *13*, 634. [CrossRef]
28. Cai, G.; Ni, H.; Li, X.; Wang, Y.; Zhao, H. Eco-Friendly Fabrication of Highly Stable Silica Aerogel Microspheres with Core-Shell Structure. *Polymers* **2023**, *15*, 1882. [CrossRef]
29. Wang, Y.; Xi, S.; Zhou, B.; Zu, G.; Liang, X.; Zhang, X.; Shen, J.; Wang, X. Superhydrophobic Highly Flexible Triple-Network Polyorganosiloxane-Based Aerogels for Thermal Insulation, Oil-Water Separation, and Strain/Pressure Sensing. *ACS Appl. Mater. Interfaces* **2024**, *16*, 30324–30335. [CrossRef] [PubMed]
30. Alves, P.; Dias, D.A.; Rodrigues Pontinha, A.D. Silica Aerogel-Rubber Composite: A Sustainable Alternative for Buildings' Thermal Insulation. *Molecules* **2022**, *27*, 7127. [CrossRef]
31. Lee, H.; Lee, D.; Cho, J.; Kim, Y.-O.; Lim, S.; Youn, S.; Jung, Y.C.; Kim, S.Y.; Seong, D.G. Super-insulating, flame-retardant, and flexible poly (dimethylsiloxane) composites based on silica aerogel. *Compos. Part A-Appl. Sci. Manuf.* **2019**, *123*, 108–113. [CrossRef]
32. Zhang, T.; Yu, D.; Xu, F.; Kong, Y.; Shen, X. Flexible Silica Aerogel Composites for Thermal Insulation under High-Temperature and Thermal-Force Coupling Conditions. *ACS Appl. Nano Mater.* **2024**, *7*, 6326–6338. [CrossRef]
33. Yoda, S.; Takeshita, S.; Ono, T.; Tada, R.; Ota, H. Development of a New Silica Aerogel-Polypropylene Foam Composite as a Highly Flexible Thermal Insulation Material. *Front. Mater.* **2021**, *8*, 74846. [CrossRef]
34. Gu, J.; Fu, R.; Kang, S.; Yang, X.; Song, Q.; Miao, C.; Ma, M.; Wang, Y.; Sai, H. Robust composite aerogel beads with pomegranate-like structure for water-based thermal insulation coating. *Constr. Build. Mater.* **2022**, *341*, 127722. [CrossRef]
35. Han, D.; Wang, C.; Han, C.B.; Cui, Y.; Ren, W.R.; Zhao, W.K.; Jiang, Q.; Yan, H. Highly Optically Selective and Thermally Insulating Porous Calcium Silicate Composite SiO_2 Aerogel Coating for Daytime Radiative Cooling. *ACS Appl. Mater. Interfaces* **2024**, *16*, 9303–9312. [CrossRef] [PubMed]
36. Mahadik, D.B.; Jung, H.-N.-R.; Han, W.; Cho, H.H.; Park, H.-H. Flexible, elastic, and superhydrophobic silica-polymer composite aerogels by high internal phase emulsion process. *Compos. Sci. Technol.* **2017**, *147*, 45–51. [CrossRef]
37. Shi, S.; Lei, B.; Li, M.; Cui, X.; Wang, X.; Fan, X.; Tang, S.; Shen, J. Thermal decomposition behavior of a thermal protection coating composite with silicone rubber: Experiment and modeling. *Prog. Org. Coat.* **2020**, *143*, 105609. [CrossRef]
38. Duong, T.H.; Margaillan, A.; Bressy, C. Thermal degradation of hydroxyalkylated poly (dimethylsiloxane)s and poly (dimethylsiloxane)-poly (trialkylsilyl methacrylate) based block copolymers synthesized by RAFT polymerization. *Polym. Degrad. Stab.* **2019**, *164*, 136–144. [CrossRef]
39. Yao, C.; Dong, X.; Gao, G.; Sha, F.; Xu, D. Microstructure and Adsorption Properties of MTMS/TEOS Co-precursor Silica Aerogels Dried at Ambient Pressure. *J. Non-Cryst. Solids.* **2021**, *562*, 120778. [CrossRef]
40. Zhang, S.; Wang, H. Thermal degradation of amino-group-modified polydimethylsiloxane. *J. Therm. Anal. Calorim.* **2011**, *103*, 711–716. [CrossRef]
41. Ibrahim, M.; Biwole, P.H.; Wurtz, E.; Achard, P. A study on the thermal performance of exterior walls covered with a recently patented silica-aerogel-based insulating coating. *Build. Environ.* **2014**, *81*, 112–122. [CrossRef]
42. He, S.; Wu, X.; Zhang, X.; Sun, J.; Tian, F.; Guo, S.; Du, H.; Li, P.; Huang, Y. Preparation and properties of thermal insulation coating based on silica aerogel. *Energy Build.* **2023**, *298*, 113556. [CrossRef]
43. Wang, P.; He, B.; An, Z.; Xiao, W.; Song, X.; Yan, K.; Zhang, J. Hollow glass microspheres embedded in porous network of chitosan aerogel used for thermal insulation and flame retardant materials. *Int. J. Biol. Macromol.* **2024**, *256*, 128329. [CrossRef] [PubMed]
44. Li, J.; Ahmad, Z.; Chen, J.; Chen, H.; Tao, J. Fabrication of SiC nanofiber aerogel felt with high-temperature thermal insulation performance. *J. Eur. Ceram. Soc.* **2024**, *44*, 1923–1931. [CrossRef]
45. Yang, M.; Lixia, Y.; Chen, Z.; Qiong, W.; Wang, Y.; Liu, T.; Li, M. Flexible Electrospun strawberry-like structure SiO_2 aerogel nanofibers for thermal insulation. *Ceram. Int.* **2023**, *49*, 9165–9172. [CrossRef]